International Journal of Biological Macromolecules 379 (2026) 153968

Contents lists available at ScienceDirect

International Journal of Biological Macromolecules

journal homepage: www.elsevier.com/locate/ijbiomac

Structural and functional insights into aromatic amino acid decarboxylase deficiency variants producing an α-synuclein-targeting L-Dopa–pyridoxal 5′-phosphate cyclic adduct

Philipp Trolese [a,b,1], Giovanni Bisello [a,1], Cristian Andres Carmona Carmona [a,2], Giulia Spagnoli [a], Alberto Benetollo [c], Doriana Sandonà [c], Laura Acquasaliente [b], Patrizia Polverino de Laureto [b,*], Mariarita Bertoldi [a,*]

[a] Department of Neuroscience, Biomedicine and Movement Sciences, University of Verona, Verona, Italy
[b] Department of Pharmaceutical and Pharmacological Sciences, University of Padova, Padova, Italy
[c] Department of Biomedical Sciences, University of Padova, Padova, Italy

ARTICLE INFO

Keywords:
Aromatic amino acid decarboxylase deficiency
Pictet-Spengler adduct
A-Synuclein
Pyridoxal 5′-phosphate

ABSTRACT

The inherent reactivity of free- or enzyme-linked pyridoxal 5′-phosphate (PLP) in the presence of catechol compounds with an aminic group is known and leads, after the formation of a Schiff base, to an irreversible cyclic adduct, called the Pictet-Spengler condensation product. In PLP-dependent aromatic amino acid decarboxylase (AADC), the protein scaffold protects PLP, preventing its leakage as a cyclic adduct complexed with the L-Dopa substrate. Here, we demonstrate that a group of AADC deficiency enzyme variants can undergo this unproductive reaction at a high rate. By using computational modeling, spectroscopic and functional studies with twelve pathogenic variants, we uncovered the basis of the variants' ability to synthesize this adduct. Since the metabolic conditions present in patients (high PLP amount as medical treatment and high L-Dopa concentrations as a consequence of enzyme impairment) may trigger Pictet-Spengler adduct synthesis, we modeled the possible oxidative effects played by this compound on α-synuclein (Syn) in solution and in neuroblastoma SH-SY5Y cells, given the known sensitivity of this protein to dopamine or dopa-related compounds. By multiple experimental approaches including chromatographic analysis, colorimetric assays, native mass spectrometry, dynamic light scattering and isothermal titration calorimetry, transmission electron microscopy, as well as cytotoxicity assays, we determined that the Pictet-Spengler adduct is not toxic to cells, exhibits a dose dependent inhibition of Syn fibrillation, and promotes Syn oxidation. These observations suggest that the AADC pathogenic variants undergoing Pictet-Spengler condensation could synthesize the biologically active adduct enhancing oxidative stress in neuronal cells, thereby contributing to the worsening of the phenotype.

1. Introduction

The formation of a cyclic tetrahydroisoquinoline adduct (also called the Pictet-Spengler condensation product) is an irreversible step of the rearrangement of the Schiff base between Dopa (either the L- or the D-enantiomer) and pyridoxal [1] or pyridoxal 5′-phosphate (PLP) [2]. In detail, the C6 of Dopa undergoes a nucleophilic attack on the imine carbon atom of the coenzyme, leading to a cyclized compound with a sp^3 configuration on C4' (Fig. 3A). In the presence of free PLP, the reaction with Dopa is fast (~ 0.2 min^{-1} [3]), irreversible, and leads to the complete conversion of PLP to the cyclic adduct [3]. In PLP-enzymes employing aromatic amino acids as substrates, the cofactor is buried in the active site, preventing or minimizing any possible side activity [4], including this irreversible non enzyme-driven reaction. The case of aromatic amino acid decarboxylase (AADC) is exemplary: mammalian AADC can undergo Pictet-Spengler condensation with D-aromatic amino acids or amines [2], while in the presence of the natural substrate L-Dopa less than 1% of the original enzyme-bound PLP is recovered as

* Corresponding authors.
E-mail addresses: patrizia.polverinodelaureto@unipd.it (P.P. de Laureto), mita.bertoldi@univr.it (M. Bertoldi).
[1] co-first authors.
[2] Present address: Department of Biology, University of Padova, Padova, Italy.

https://doi.org/10.1016/j.ijbiomac.2026.153968
Received 28 April 2026; Received in revised form 4 August 2026; Accepted 5 August 2026
Available online 7 August 2026
0141-8130/© 2026 The Authors. Published by Elsevier B.V. This is an open access article under the CC BY license (http://creativecommons.org/licenses/by/4.0/).

Pictet-Spengler adduct [5] with a calculated exponential rate constant of about 0.02 min^{-1} [6]. This behavior witnesses how the protein scaffold maintains PLP reaction intermediates at the active site, protecting them from solvent exposure and keeping them in a closed conformation to ensure efficient catalysis [7]. The fact that even wild-type (WT) AADC can produce a small amount of cyclic adduct is an inevitable consequence of the reactivity and versatility of the PLP coenzyme.

Active site variants of human AADC, built to study the role of the corresponding residues at the binding/catalytic cleft, display an enhanced rate of Pictet-Spengler condensation than WT. This is due to a structural damage at the active site, which prevents the enzyme from reaching a catalytically competent conformation, and leaves the external aldimine intermediate insufficiently shielded to proceed with catalysis, instead escaping as a stable cyclic adduct [8–10].

Interestingly, the formation of the cyclic adduct is not restricted to artificial AADC variants. Some (but not all) pathogenic human AADC variants (p.Ala91Val, p.Gly102Ser, p.Ala110Glu, p.Ser147Arg, p.Phe309Leu, p.Pro330Leu and p.Leu353Pro), causing the severe neurotransmitter rare disease AADC deficiency [11,12], were reported to be able to synthesize it [3,6,13,14] at rate comparable to (2-fold increase) or even exceeding (5-fold increase) that of the WT, leading to PLP irreversible depletion. The rationale for this behavior has not yet been determined, although the resolution of the crystal structure of the human AADC enzyme in the external aldimine conformation, with a closed active site, may shed light on the requirement for active site integrity to prevent nonenzymatic reactions [7].

The fact that some AADC deficiency variants can synthesize the adduct is particularly interesting, given that all patients are supplemented with pyridoxine, the precursor of PLP, yet not all derive clinical benefit from this dietary intervention [11]. To the best of our knowledge, the Dopa-PLP cyclic adduct has never been investigated as a possible biomarker for some clusters of variants. In addition, its highly oxidation-prone chemical features have never been characterized.

To monitor its effects, if endogenously synthesized, we chose α-Synuclein (Syn) as a target. Syn is mainly localized in the same presynaptic nerve terminals of AADC, and is predominantly abundant in the central nervous system (CNS) where it is involved in synaptic vesicle trafficking, neurotransmission, and synaptic plasticity [15]. It was shown that Syn co-immunoprecipitates with AADC in rat striatum [16]), thereby reducing its activity. This implies that reduction of local concentration of Syn, whether due to reduced expression or aggregation, may lead to selectively disruption of DA homeostasis. In addition, some catabolites of dopamine such as 3,4-dihydroxyphenylacetaldehyde (DOPAL), 3,4-dihydroxyphenylacetic acid (DOPAC), and 3,4-dihydroxyphenyl ethanol (DOPET) affect Syn aggregation and its neurotoxic properties [17–20]. Notably, L-Dopa catabolites alone have been shown to react *via* a similar condensation mechanism with acetaldehyde, to form salsolinol, which has been detected in the urine of Parkinson's Disease patients [21]. Syn represents the major proteinaceous component of aggregates that constitute the neuropathological hallmarks of several neurodegenerative diseases known as α-synucleinopathies, including Parkinson's disease, dementia with Lewy bodies, and multiple system atrophy [22]. Interestingly, AADC deficiency also belongs to the group of infantile Parkinsonism-dystonia disorders for symptoms, even though it is not a neurodegenerative disease [23].

Since the reaction of AADC with L-Dopa is faster (on the order of magnitude of s^{-1}) than the irreversible condensation of free PLP with L-Dopa (on the order of magnitude of min^{-1}), we focused our attention on the loss-of-function AADC variants for their ability to synthesize the Dopa-PLP cyclic adduct, given their impacted decarboxylase reaction. Furthermore, we investigated the biological effects of this compound on Syn in neuroblastoma SH-SY5Y cells, leading to a new interpretation of the effects of vitamin B_6 supplementation and paving the way for further diagnostic and pharmacological treatments.

2. Experimental section

2.1. Chemicals

PLP, L-Dopa (Merck), Thioflavin T (ThT) and other chemicals and reagents were of analytical grade and were obtained from Merck (Darmstadt, Germany). Bicinchoninic acid (BCA) assay kit, fetal bovine serum and DMEM/F-12 HEPES medium (Cat. No. 31330–038) were purchased from Thermo Fischer Scientific (Waltham, Massachusetts, USA). Neuroblastoma SH-SY5Y cells were obtained from AATC (LGC Standards S.r.l., Italy). Membrane soluble tetrazolium salt (MTS) reagent kit (CellTiter 96® AQueous One Solution Cell Proliferation Assay) was obtained from Promega, Madison, WI, USA. OZBlue cell viability kit was purchased from OZ Biosciences, San Diego, CA 92126, USA.

2.2. Synthesis and characterization of the Pictet-Spengler adduct

The PLP-L-Dopa adduct was synthesized by adding 2 mM L-Dopa to different PLP concentrations (1–100 μM) and following the decrease of absorbance at 388 nm (free PLP) and the increase at 328 nm, typical of a C4' sp^3 species in 100 mM potassium phosphate buffer, pH 7.4 [2]. The calculated molar extinction coefficient is 7076 M^{-1} cm^{-1}. For the adduct synthesis and purification, PLP and L-Dopa were incubated at a 1:4 M ratio (2.5 mM PLP and 10 mM L-Dopa) in 100 mM potassium phosphate buffer (pH 7.4) at 37 °C with shaking at 300 rpm. Reaction progress was monitored using a Jasco V-750 spectrophotometer by following the disappearance of the PLP absorbance band at 388 nm. After 1 h, the reaction was quenched by addition of 10% (*w/v*) trichloroacetic acid (TCA). The mixture was injected multiple times onto a Gemini C18 column (150 Å, 4.6 mm, Phenomenex, CA, USA) using a Jasco PU-2080 Plus HPLC system equipped with a UV-1570 detector set at 295 nm. Initial purification was performed using water as the mobile phase at a flow rate of 1 mL/min. Under these conditions, the Pictet–Spengler adduct eluted at 6 mL, while free L-Dopa eluted at 8 mL. Collected fractions containing the adduct were lyophilized, resuspended in water, and quantified spectrophotometrically using 7076 M^{-1} cm^{-1} at 328 nm. Purity was assessed with the same Gemini C18 column with 100 mM potassium phosphate (pH 2.35) as mobile phase. The adduct elutes as a single peak and is >95% pure. The PLP-Dopa adduct has already been identified by nuclear magnetic resonance analysis [2,3].

2.3. Cloning, expression, and purification of recombinant AADC deficiency variants

AADC variants (p.Tyr20del, p.His70Arg-Trp71del, p.Trp105Cys, p.Gly146Arg) were obtained by site-directed mutagenesis as described [3]. The appropriate oligonucleotides (**Table S1**) and their complements were used for each mutagenesis reaction employing the Quick-Change II kit (Agilent Technologies). The mutations were confirmed by DNA sequence analysis of the whole ORF. Variants p.Ala110Glu, p.Pro330Leu, p.Arg347Gln and p.Leu353Pro are already available [3,14,24]. Expression and purification have been carried out as described [3].

2.4. Alpha-fold structural models of WT and variant AADC enzymes

The human AADC crystal structure (pdb:8ora) was used as template. Several independent *in silico* approaches were used to evaluate the effects of the AADC variants on protein stability $\Delta\Delta G_{fold}$ (FoldX [25], DynaMut2 [26], DUET [27]). For FoldX calculations, the mutations were introduced simultaneously in both subunits with five BuildModel runs, while for DynaMut2 and DUET analyses were performed using their standard workflows. Positive FoldX ΔΔG values and negative DynaMut2 and DUET scores indicate decreased protein stability compared to the WT. In-frame deletion variants p.Try20del and p.His70Arg/Trp71del models were generated using AlphaFold [28] together with WT dimeric AADC for comparative analysis. WT model was evaluated by comparing

the root mean square deviations (RMSD) with respect to the crystal structure (pdb:8ora). Thereafter, the stability of unfolding (ΔG_{fold}) of these AlphaFold models was then analyzed using FoldX. Images were rendered by the software PyMOL (Version 2.2.3, Schrödinger, Limited Liability Company; New York, NY, USA).

2.5. Expression and purification of Syn

Recombinant Syn was produced in *Escherichia coli* BL-21 following an established purification procedure previously reported by [17]. After cell harvesting, periplasmic extraction was performed and the soluble fraction was subjected to heat treatment, ammonium sulfate fractionation (50% saturation), and ion-exchange chromatography. The identity and molecular integrity of the purified protein were verified by mass spectrometric analysis.

2.6. Chromatographic analyses

2.6.1. Reverse phase (RP)-HPLC analyses of coenzyme modification and activity measurement for AADC deficiency variants

AADC variants were incubated at 10 μM protein concentration with 2 mM L-Dopa in 100 mM potassium phosphate buffer, pH 7.4 at 25 °C. Concentration-time curves were followed by withdrawing aliquots at time intervals and quenching the reaction by adding trichloroacetic acid to a final concentration of 10% (*w/v*). Proteins were then precipitated in ice and removed by centrifugation. Supernatants were analyzed by HPLC as described [5] using a Gemini C18 column (150 Å, ~ 4.6 mm, Phenomenex, CA, USA) and performed on a Jasco PU-2080 Plus HPLC system equipped with a UV-1570 detector set at 295 nm. Samples were eluted in 50 mM potassium phosphate, pH 2.35, at a flow rate of 1 mL/min. Standard curves of peak area as a function of coenzyme or cyclic adduct concentration were prepared with commercially available PLP and coenzyme adducts obtained by synthesis (see Results section). Activity was determined at 2 mM L-Dopa concentration in triplicate with the procedure already reported [14] and quantified by determining the initial rate PLP decay or cyclic adduct increase.

2.6.2. RP-HPLC of Syn in the presence of the Pictet-Spengler adduct

Unless otherwise stated RP-HPLC analysis of Syn were carried out as described elsewhere [17]. Syn samples collected from the aggregation mixture at pH 7.4 were centrifuged, injected into a Jupiter C18 column (4.6 × 250 mm, 5.0 μm; Phenomenex, Torrence, CA, USA) and eluted using a water/acetonitrile 0.1% trifluoracetic acid gradient of 5 to 38% in 5 min and 38 to 43% in 15 min measuring at a wavelength of 226 nm. Identity of protein species collected under the peaks was controlled by electrospray ionization (ESI) mass spectrometry (MS) on a Xevo® G2-XS ESI-Q-TOF mass spectrometer (Waters Corporation, Milford, MA, USA).

2.7. ThT binding assay of the Pictet-Spengler adduct with Syn

The formation of amyloid-like aggregates was monitored using Thioflavin T (ThT) fluorescence. At each sampling time, 15 μL of aggregation mixture was added to 235 μL of 25 μM ThT prepared in 20 mM sodium phosphate buffer (pH 6.0). Fluorescence spectra were acquired at 25 °C using an excitation wavelength of 440 nm and collecting emission between 450 and 600 nm. Control measurements containing only the Pictet–Spengler adduct were recorded to evaluate possible interference with the fluorescent signal. Data are reported as the mean value of three replicates ± standard deviation (SD).

2.8. BCA assay for quantifying protein amount

The BCA assay was performed on a NanoDrop system. The fresh BCA working reagent was prepared using a 50:1 ratio of the kit reagents A:B. The calibration curve was measured by using bovine serum albumin at different concentrations (0, 0.25, 0.5, 0.75 and 1 mg/mL) as a standard. For each standard/sample 10 μL of solution/supernatant were mixed with 200 μL BCA working reagent mixture. Standards and samples were incubated at 37 °C for 30 min and then cooled to room temperature. The absorbance of the BCA/copper complex was measured at 562 nm. For the measurement 2 μL of sample were used.

2.9. Aggregation kinetics and isolation of Syn components during aggregation

Syn aggregation in the presence or absence of the Pictet-Spengler adduct was monitored by checking for ThT fluorescence, circular dichroism (CD) spectroscopy and concentration of soluble protein at different time points (0 h, 48 h, 96 h and 168 h) for seven days as described above. Syn at 70 μM (1 mg/mL) concentration (total volume = 300 μL) in 20 mM sodium phosphate buffer (pH 7.4 and pH 6) was incubated in a 1.5 mL microcentrifuge tube at 37 °C under agitation (700 rpm) for each time point under different conditions: Syn alone, Syn with 70 μM Pictet-Spengler adduct (1:1) and Syn with 350 μM Pictet-Spengler adduct (1:5). In addition, as a control samples of 70 μM and 350 μM of the cyclic adduct alone were put under the same treatment. Briefly, at each time point an aliquot (15 μL) was taken for the ThT measurement. The rest was centrifuged at 15000 rpm for 30 min to pellet down the fibril fraction and separate the monomeric Syn in the supernatant. The amount of formed fibrils was determined by subtracting the concentration of protein left in the supernatant from the initial protein concentration. For the samples containing only Syn the concentration was determined by absorption measurements at 280 nm using a double-beam Jasco V-730 spectrophotometer. The molar absorptivity (ε) of Syn is 5960 M^{-1} cm^{-1}. For the samples containing Syn and the Pictet-Spengler adduct, the concentration was measured performing a BCA assay with a Nanodrop system. BCA assay was also done with the samples containing only Syn alone. Since the Pictet-Spengler adduct interferes both with UV-spectrophotometry at 280 nm and with the BCA assay, the concentration measured for the samples containing Syn and the adduct was always corrected by subtracting the contribution from the Pictet-Spengler adduct obtained by performing a BCA assay on samples only containing 70 μM and 350 μM adduct. To check if at the aggregation time point oxidized forms of Syn were present, the aggregation mixtures at pH 6 and pH 7.4 were buffer exchanged with water with centrifugal filters and analyzed with mass spectrometry.

2.10. Circular dichroism (CD) spectroscopy of AADC variants and Syn

Near UV–visible CD spectral measurements of AADC deficiency variants were recorded at an enzyme variant concentration of 5 μM in 100 mM potassium phosphate, pH 7.4, at 25 °C with a Jasco J-710 spectropolarimeter at a scan speed of 50 nm/min, bandwidth of 2 nm in the presence of 10 μM exogenous PLP. Far UV CD measurements of Syn were conducted as described previously unless otherwise stated [29]. Briefly, supernatants of the centrifuged aggregation mixtures were diluted to obtain a concentration of 7 μM. The pellets on the other hand were resuspended in 200 μL, which is the minimal volume needed for the CD measurement. Data were collected in the wavelength range of 195–250 nm. Five accumulations were measured for all samples, which were successively averaged and blank subtracted. From the samples containing the Pictet-Spengler adduct, a blank containing 70 μM and 350 μM adduct diluted in the same way as their corresponding supernatant was subtracted. Only data with high tension voltage <600 V were collected to avoid too noisy signals. The mean residue ellipticity [θ] (degree cm^2 $dmol^{-1}$ $residue^{-1}$) was calculated from the following Eq. [30]:

$$[\theta] = \frac{\theta_{obs}}{10} \cdot \frac{MRW}{lc} \quad (1)$$

where θ_{obs} is the observed ellipticity in degrees; MRW is the mean residue molecular weight of the protein (g/mol), l in the optical path length (cm) and c is the protein concentration (g/mL).

2.11. Transmission electron microscopy (TEM)

Aggregate morphology was examined after 192 h of incubation by transmission electron microscopy. Samples were deposited onto Butvar-coated 400-mesh copper grids and negatively stained with 1% (*w/v*) uranyl acetate. Images were collected using a Tecnai G2 12 Twin microscope (FEI, Hillsboro, OR, USA) operated at 100 kV.

2.12. Dynamic light scattering (DLS)

Particle size distributions were determined by dynamic light scattering using a Zetasizer Ultra instrument (Malvern Instruments, UK). Samples were analyzed in UV-transparent disposable cuvettes with a 0.45 cm optical path. Instrument attenuation was automatically optimized during acquisition. Measurements were performed in triplicate and processed using ZS Xplorer software, with results reported as number-weighted distributions. Data on particle size are reported as mean ± SD of a triplicate, each one consisting of 30 repetitions.

2.13. Native mass spectrometry (native MS)

Native MS measurements were carried out using the same instrument setup and general workflow as described previously [17]. In brief, prior to analysis, Syn and Syn incubated with 350 μM Pictet–Spengler adduct were subjected to purification by size exclusion chromatography (SEC) using a Superdex™ 200 Increase 10/300 GL column (Amersham Biosciences, Uppsala, Sweden). Following SEC, the proteins were exchanged into 200 mM ammonium acetate buffer (pH 7.0) and concentrated to a final protein concentration of 10 μM using Amicon Ultra-0.5 centrifugal filters (Merck Millipore, Ireland).

Samples were introduced by direct-infusion electrospray ionization (ESI) on a Xevo G2-S Q-Tof mass spectrometer (Waters). Measurements were carried out in nanoflow ESI mode using in-house pulled quartz emitters prepared with a P2000 laser pipette puller (Sutter Instruments, Novato, CA, USA). Each emitter was loaded with up to 5 μL of sample using gel-loading pipette tips, and a stainless-steel wire inserted at the rear of the emitter was used to apply an ionization voltage between 1.0 and 1.6 kV. The source temperature was maintained at 30 °C, with a desolvation voltage set to 40 V. All spectra were acquired in positive ion mode.

Data analysis was performed using MassLynx software (v4.2, SCN781; Waters). The relative populations of conformational states were determined by integrating the signal intensities corresponding to each species across datasets. Quantification was carried out using custom MATLAB scripts (R2016b), and results were expressed as percentage distributions to enable comparison between experimental conditions.

2.14. Isothermal titration calorimetry (ITC)

Thermodynamic characterization of the interaction between Syn and the Pictet–Spengler adduct was performed using a VP-ITC microcalorimeter (Malvern Panalytical). Protein solution (70 μM) was placed in the sample cell and titrated with 1 mM adduct solution through 27 sequential injections of 5 μL separated by 480 s intervals. Experiments were conducted in 20 mM phosphate buffer (pH 7.4) at 25 °C. Heat contributions arising from ligand dilution were measured independently and subtracted from the raw thermograms.

2.15. Cytotoxicity assays with Syn in the presence of the Pictet-Spengler adduct

Cytotoxicity of Syn in both oligomeric and fibrillar states was assessed using the human neuroblastoma SH-SY5Y cell line. Cells were cultured in DMEM/F-12 HEPES medium (Cat. No. 31330–038, Thermo Fisher Scientific, Waltham, MA, USA) supplemented with 10% fetal bovine serum (FBS; Thermo Fisher Scientific), 2 mM L-glutamine, and antibiotics (100 U/mL penicillin and 100 μg/mL streptomycin), and maintained at 37 °C in a humidified atmosphere containing 5% CO_2. For experimental treatments, cells were seeded in 96-well plates at a density of 10,000 cells per well and allowed to adhere for 24 h. The culture medium was then replaced with medium containing 1% FBS to minimize serum-related interference in toxicity measurements.

Cells were exposed to 7.0 μM Syn oligomers or fibrils, either in the absence or presence of 350 μM Pictet–Spengler adduct. Cell viability was evaluated after 24 and 48 h of incubation using the MTS assay (CellTiter 96® AQueous One Solution Cell Proliferation Assay, Promega, Madison, WI, USA). Briefly, 20 μL of MTS reagent was added to each well, followed by incubation for 2–4 h at 37 °C and 5% CO_2 according to the manufacturer's instructions. Absorbance was measured at 492 nm, corresponding to the formation of formazan by metabolically active cells. Results are presented as mean ± SD from a single experiment performed in sextuplicate.

The cytotoxicity of Pictet-Spengler adduct was tested as cell viability assay using the OZBlue cell viability assay (OZ Biosciences) [24]. Briefly, SH-SY5Y cells were seeded in 96-well plates at a density of 15×10^3 cells per well and treated with varying concentrations of the adduct for 24 or 48 h. Following treatment, 5 μL of OZBlue reagent was added to each well and cells were incubated for 1 h under standard culture conditions. Fluorescence was then recorded at 590 nm with excitation at 560 nm using a multimode microplate reader (GENios; Tecan). Data are reported as mean ± SD from three independent experiments.

3. Results

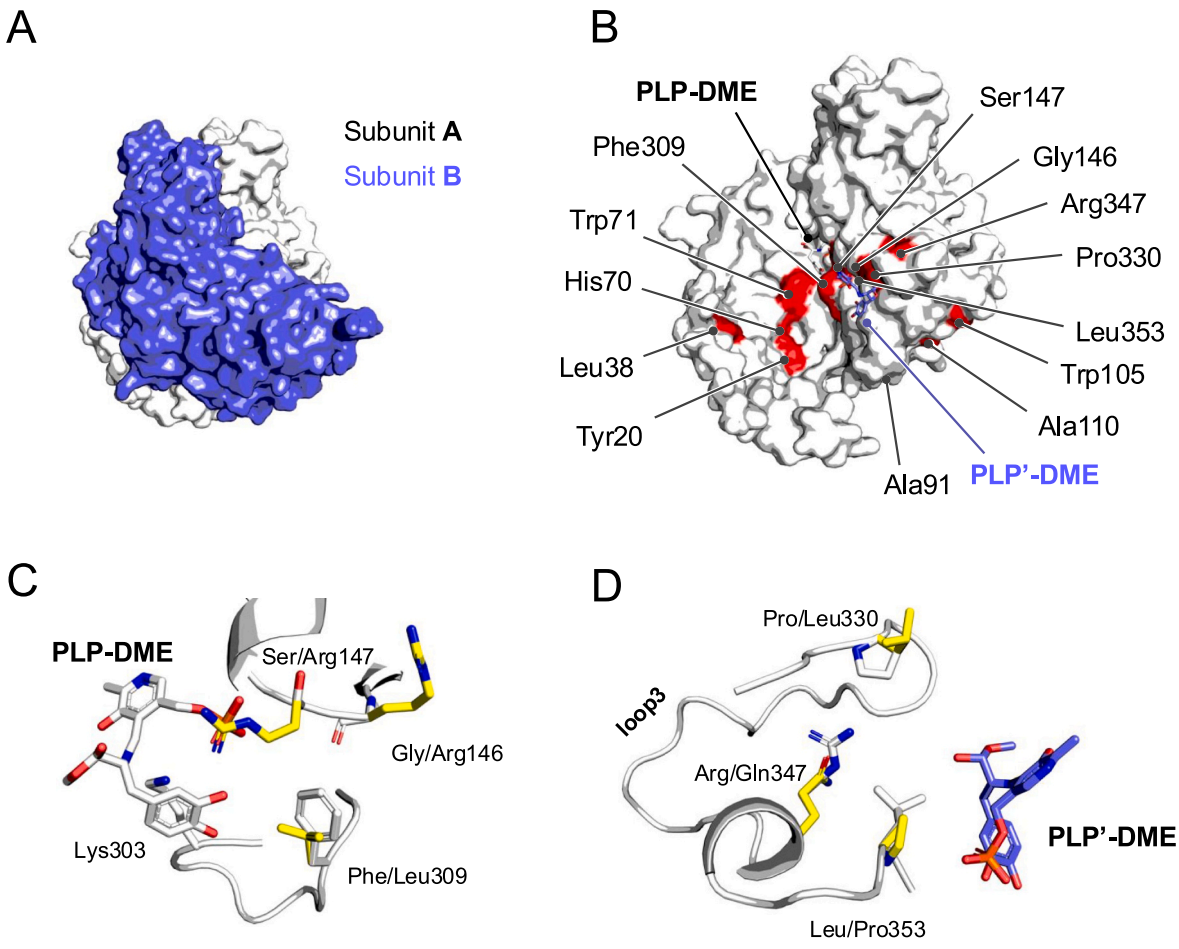
3.1. Predicted structural effects of the AADC deficiency variants by in silico analyses

We selected loss-of-function AADC deficiency variants (residual decarboxylase activity ≤ 2% (Table 1)) from the literature [3,6,13,14,31] and from the Pediatric Neurotransmitter Database (PND) for AADC deficiency (Biopku) (https://www.biopku.org/pnd/). The selected variants refer to amino acids spread at the interface between the two identical monomers composing the AADC functional dimer (Fig. 1A,

Table 1
Residual activity of AADC deficiency variants measured in the presence of saturating L-Dopa concentrations.

#	Residual decarboxylase activity (%)	Initial rate of Pictet-Spengler adduct formation (min^{-1})[a]
WT	100 ± 0.1	<0.002
p.Tyr20del	0.26 ± 0.01	0.050 ± 0.004
p.Leu38Pro	0.013 ± 0.002	0.035 ± 0.002
p.His70Arg/Trp21del	0.012 ± 0.001	0.047 ± 0.003
p.Ala91Val	0.0085 ± 0.0005	0.028 ± 0.004
p.Trp105Cys	0.046 ± 0.003	0.025 ± 0.003
p.Ala110Glu	0.0013 ± 0.0004	0.033 ± 0.003
p.Gly146Arg	1.4 ± 0.1	0.025 ± 0.003
p.Ser147Arg	0.05 ± 0.01	0.073 ± 0.005
p.Phe309Leu	2.4 ± 0.4	0.09 ± 0.01
p.Pro330Leu	0.67 ± 0.03	0.007 ± 0.001
p.Arg347Gln	0.14 ± 0.01	0.012 ± 0.002
p.Leu353Pro	0.015 ± 0.001	0.003 ± 0.002

[a] The initial rate of 10 μM free PLP in the presence of 2 mM L-Dopa is 0.2 min^{-1}. Values are reported as the mean ± SD of three independent experiments.



(caption on next page)

Fig. 1. Localization of the AADC residues involved in pathogenic substitutions and *in silico* mutagenesis. **(A)** Dimeric AADC structure (pdb:8ora) is shown as surface, and the two subunits A and B are colored in white and blue, respectively. **(B)** The localization of residues involved in the pathogenic substitutions is highlighted in red on subunit A. The PLP-DME external aldimine is shown with sticks and colored in white (subunit A) and blue (PLP'-DME, subunit B; the prime denotes a residue or the coenzyme belonging to the neighboring subunit). **(C)** Residues Gly146, Ser147, and Phe309 belonging to the same subunit of the conserved PLP-binding residue Lys303 are shown together with the PLP-DME. WT protein is colored in white; substituted residues obtained using FoldX are colored in yellow. The active-site pocket is shown with a grey circle for simplicity. **(D)** PLP'-DME of subunit B is shown together with residues Pro330, Arg347, and Leu353 belonging to loop3 of subunit A. Loop3 is indicated. **(E)** Residues Trp105' and Ala110' of subunit B and Leu38 are shown together with PLP-DME. Loop2 is indicated. **(F)** AlphaFold models of WT (green) and p.Tyr20del (yellow) are superposed and compared to the crystal structure of WT AADC (white, pdb:8ora). The RMSD between the structures is reported. The effect of the deletion on the pitch and rise of helix1 is shown. **(G)** The AlphaFold model of p.His70Arg/Trp71del (cyan) is superposed on AlphaFold model of the WT (green) and of the crystallographic WT (white, pdb:8ora). The RMSD between the structures is reported. Residues are shown as sticks. (For interpretation of the references to colour in this figure legend, the reader is referred to the web version of this article.)

B). The predicted effects of the missense variants obtained from the computational tools (FoldX, DynaMut2 and DUET) show that all of them are destabilizing (Table 2). To model the structural modifications of the substituted variants, we carried out *in silico* mutagenesis.

First, we examined the residues located at/near the PLP binding site: Gly146 and Ser147 are involved in the anchoring of the phosphate group of PLP [7], represented in its external aldimine conformation with the L-Dopa analog dopa methylester (DME), while Phe309 is in contact with residues directly binding the catechol moiety of the substrate [6], as shown in Fig. 1C. The p.Ser147Arg and p.Gly146Arg variants are predicted to cause increased steric hindrance and a change in polarity, affecting the active site of the same subunit by, as well as the dimer interface. Interestingly, Gly146 maps in a central cavity of AADC between the two active sites [7], and substituted arginine could be placed in this cavity, explaining the smaller ΔΔG with respect to p.Ser147Arg (Table 2). p.Phe309Leu may induce a local perturbation, with a possible effect on substrate binding site. Notably, the PLP-binding lysine (Lys303) of the resting enzyme maps upstream on the same loop, and could be affected by the Phe309-to-Leu substitution (Fig. 1C).

Pro330, Arg347, and Leu353 belong to loop3, a flexible motif containing the catalytically essential residue Tyr332 [7]. During catalysis, loop3 of one subunit closes upon the neighboring active site of the other subunit to properly position Tyr332 for the decarboxylase reaction (Fig. 1D, [7]). The effects of the p.Pro330Leu, p.Arg347Gln, and p.Leu353Pro variants have been already described [14,24] and do not seem strictly related to a structural alteration, rather to an overall reduced mobility of the catalytic loop [7].

Trp105 maps on loop2, a structural element of the neighboring subunit associated with substrate binding. Its substitution to Cys would affect the flexibility of loop2 with effects similar to those of the variants mapping on loop3 (Fig. 1E).

On the contrary, p.Leu38Pro, p.Ala91Val, and p.Ala110Glu may differently cause a strong perturbation of the bulky microenvironment of the secondary structural elements to which they belong (Fig. 1E). These effects are due to the increased steric hindrance introduced with Ala-to-Val and Ala-to-Glu substitutions and to the disruptive effect of the Leu-to-Pro substitution on the helical structure.

The variants characterized by an amino acid deletion, p.Tyr20del and p.His70Arg/Trp71del, were modeled using AlphaFold, and their stability was evaluated with FoldX (Fig. 1F, G and Table 2). In frame deletion of Tyr20 is predicted to alter helix1 (residue 1–25) geometry with reduced pitch and rise of downstream region 19–25 compared to WT (Fig. 1F). The AlphaFold model of p.His70Arg/Trp71del shows that the overall backbone of loop1 (residues 66–84) is altered, and that deletion of Trp71 would result in the loss of a short motif harboring Trp71 (involved in substrate hydrophobic stabilization) and His72 (Fig. 1G).

Overall, p.Tyr20del and p.His70Arg/Trp71del are predicted to affect structural elements, as p.Leu38Pro, p.Ala91Val, and p.Ala110Glu.

3.2. Incompetent AADC deficiency variants with altered PLP microenvironment synthesize the Pictet-Spengler adduct

All the purified variants are folded since they exhibit far UV CD spectra similar to that of the WT (data not shown). However, they differ in the extent of decrease of the dichroic band at 280 nm compared with the WT. Some variants showed almost no (p.Pro330Leu and p.Arg347Gln) or slight changes (p.Trp105Cys, p.Gly146Arg, p.Ser147Arg, p.Phe309Leu, and p.Leu353Pro), whereas others exhibited pronounced decreases (p.Tyr20del, p.Leu38Pro, p.His70Arg-Trp71del, p.Ala91Val, p.Ala110Glu) (Fig. 2A). This band reflects the environment of buried aromatic amino acids and serves as an indication of tertiary structure. Thus, variants with a markedly reduced or absent band appear to have more compromised tertiary conformations relative to the WT. Interestingly, the calculated $\Delta\Delta G_{fold}$ of missense variants (Table 2) shows a correlation with the measured dichroic signal at 280 nm ($r = -0.817$), suggesting that variants predicted to be more destabilizing (p.Leu38Pro, p.Ala91Val, and p.Ala110Glu) also show higher structural alterations in solution (Fig. 2B).

Changes in the aromatic environment are accompanied by

Table 2
Predicted stability effects of the AADC variants using independent computational approaches.

#	FoldX (dimer) $\Delta\Delta G_{fold}$ (kcal/mol)	DUET $\Delta\Delta G_{fold}$ (kcal/mol)	DynaMut2 $\Delta\Delta G_{fold}$ (kcal/mol)	FoldX ΔG_{fold} AlphaFold model (kcal/mol)	Overall prediction
WT (AlphaFold model)				−281.4	
p.Tyr20del	nd	nd	nd	−279.1	destabilizing
p.Leu38Pro	21.5 ± 2.3	−1.737	−0.98		destabilizing
p.His70Arg/Trp71del	nd	nd	nd	−263.7	destabilizing
p.Ala91Val	20.2 ± 0.5	−0.466	−1.13		destabilizing
p.Trp105Cys	10.9 ± 0.1	−2.023	−2.22		destabilizing
p.Ala110Glu	13.0 ± 2.6	−2.841	−1.15		destabilizing
p.Gly146Arg	−0.13 ± 0.98	−0.774	−0.77		destabilizing
p.Ser147Arg	11.3 ± 0.6	−0.04	0.07		destabilizing
p.Phe309Leu	0.29 ± 0.04	−1.476	−1.83		destabilizing
p.Pro330Leu	4.6 ± 0.3	−0.333	−0.47		destabilizing
p.Arg347Gln	0.47 ± 0.42	−1.502	−0.62		destabilizing
p.Leu353Pro	7.4 ± 0.1	−1.698	−0.85		destabilizing

nd, not determinable.

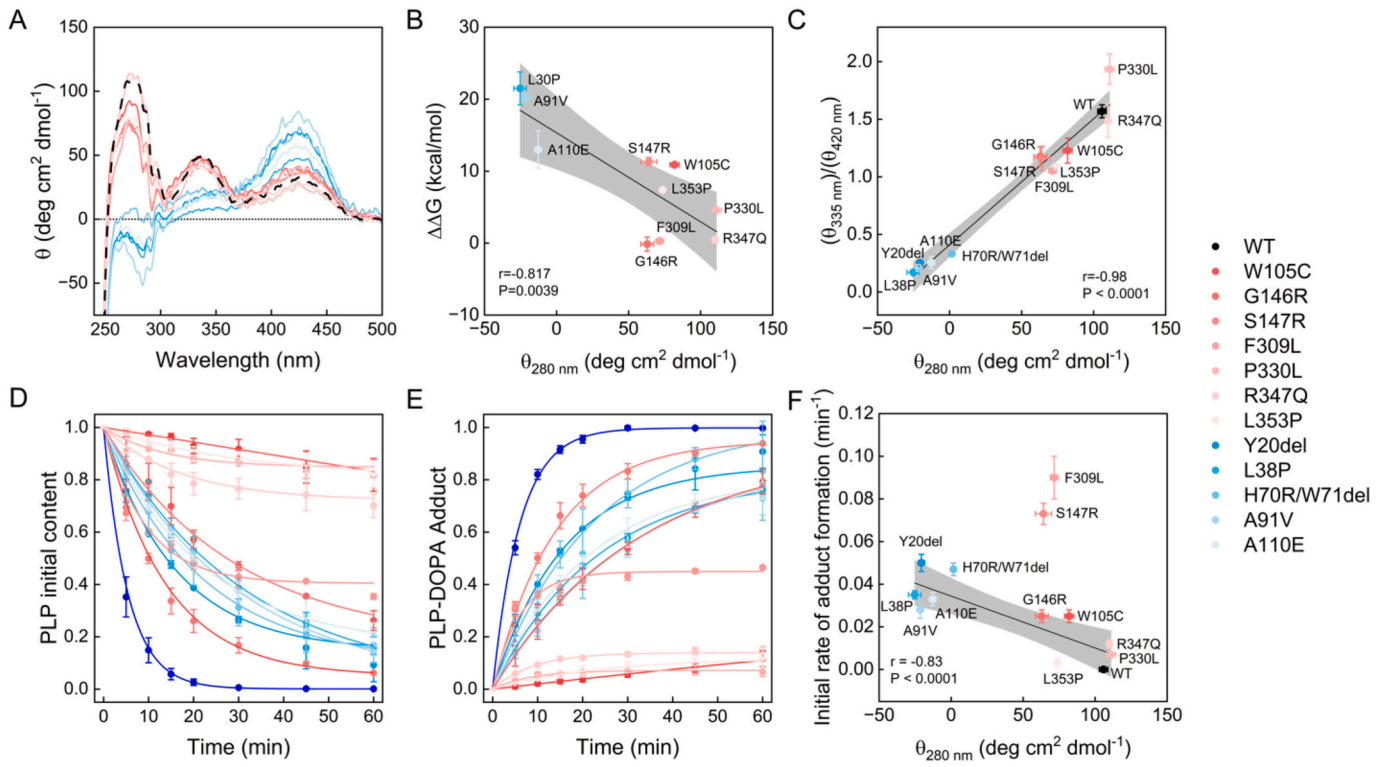


Fig. 2. Near UV–Vis CD spectra and coenzyme modifications during the reaction of AADC deficiency variants with L-Dopa. Variants are colored-coded as either highly structurally affected (red) or minimally/not structurally affected (blue). The colour shades are consistent with the localization of the variant on the AADC primary sequence (from darker to lighter red or blue colors referred to amino acids located from the amino to the carboxy terminal). The colors shading is shown at the right of the panels. **(A)** Near UV–Vis CD spectra of AADC deficiency variants at a concentration of 5 μM in 100 mM potassium phosphate buffer, pH 7.4, at 25 °C (WT AADC is reported as a reference, dashed line). **(B)** Correlation plot of the dichroic signal at 280 nm and the predicted $\Delta\Delta G_{fold}$ (Table 2). **(C)** Correlation plot of dichroic signals at 280 nm and the dichroic ratio 335/420 nm for each AADC variant. The decrease of PLP **(D)** and the increase of the Pictet-Spengler adduct **(E)** were monitored during the reaction of AADC deficiency variants (10 μM) with L-Dopa (2 mM) in 100 mM potassium phosphate buffer, pH 7.4, at 25 °C by RP-HPLC. Data for the variants are colored according to the legend. The control containing free PLP and DOPA is colored in dark blue. **(F)** Correlation plot of the rate of adduct formation *versus* the dichroic signal at 280 nm for each AADC variant.
All symbols represent the mean value of three replicates, and the error bars represent SD. In the correlation plots the grey-shaded area refers to 95% confidence interval. All Pearson coefficients and *P* values were determined with Prism, 8.4.0 (GraphPad). (For interpretation of the references to colour in this figure legend, the reader is referred to the web version of this article.)

alterations in the PLP microenvironment, as evidenced by a shift in the internal aldimine tautomeric equilibrium toward the ketoenamine form in the five most affected variants (Fig. 2A**).** There is a strong correlation ($r = 0.98$) between the dichroic signal at 280 nm and the 335/420 nm dichroic ratio (Fig. 2C). This suggests that an alteration in the protein folding is strongly associated to an alteration in the PLP binding pocket.

In the presence of L-Dopa, all these loss-of-function variants undergo Pictet-Spengler condensation reaction, clustering in two groups characterized by a faster (p.Tyr20del, p.Leu38Pro, p.His70Arg-Trp21del, p.Ala91Val, p.Ala110Glu, and p.Gly146Arg, p.Ser147Arg, p.Phe309Leu) or slower (p.Trp105Cys, p.Pro330Leu, p.Arg347Gln and p.Leu353Pro) rate of PLP-L-Dopa cyclic adduct formation (Fig. 2D,E **and** Table 1). The anomalous behavior of p.Phe309Leu variant is due to its decarboxylase rate leading to L-Dopa consumption in about 15–20 min, thereby stopping PLP condensation reaction with L-Dopa.

Overall, the variants that are more prone to release their coenzyme as cyclic adduct with L-Dopa are also those showing the most marked alterations in spectroscopic features (**Fig. 2F**, r = −0.83), with the exception of p.Ser147Arg and p.Phe309Leu which retain their spectroscopic features, but synthesize the Pictet-Spengler adduct at high rates. It can be inferred that these variants, although not particularly affected from a structural point of view, push the synthesis of the irreversible adduct, since the modifications introduced directly disturb PLP and substrate stabilization.

3.3. Production and characterization of the Pictet-Spengler cyclic adduct

The Pictet-Spengler adduct was successfully generated by nonenzymatic condensation of L-Dopa and PLP and purified as described in the Materials and Methods. We first evaluated the chemical stability of the cyclic compound under different experimental conditions. Upon prolonged incubation (up to 168 h) in 20 mM sodium phosphate buffer at pH 7.4, an additional absorption band is visible in the UV–Vis spectrum at approximately 420 nm (Fig. 3B**, top**). This observation indicates that the dominant chemical behavior of the compound is governed by its catechol functionality, suggesting that the cyclic adduct behaves primarily as a free catechol in solution. Notably, the intensity of the 420 nm band is lower at higher compound concentrations compared to 70 μM **(**Fig. 3B**, bottom)**, consistent with a concentration-dependent shift toward rapid secondary reactions that consume quinones intermediates through polymerization. This behavior places the Pictet-Spengler adduct in the same reactivity class as dopamine, DOPAC, and DOPAL, which are known to undergo auto-oxidation at pH values above 7, generating quinones and reactive oxygen species [32,33]. The yellowing of the solution observed over time is in agreement with this oxidative chemistry. Mass spectrometric analysis further supports this interpretation: while freshly purified PLP-Dopa adduct displays the expected *m/z* of 427, prolonged incubation at pH 7.4 does not result in a discrete quinone species (m/z 425), but rather in the formation of heterogeneous polymerized products (Fig. 3C). This behavior is consistent with catechol-

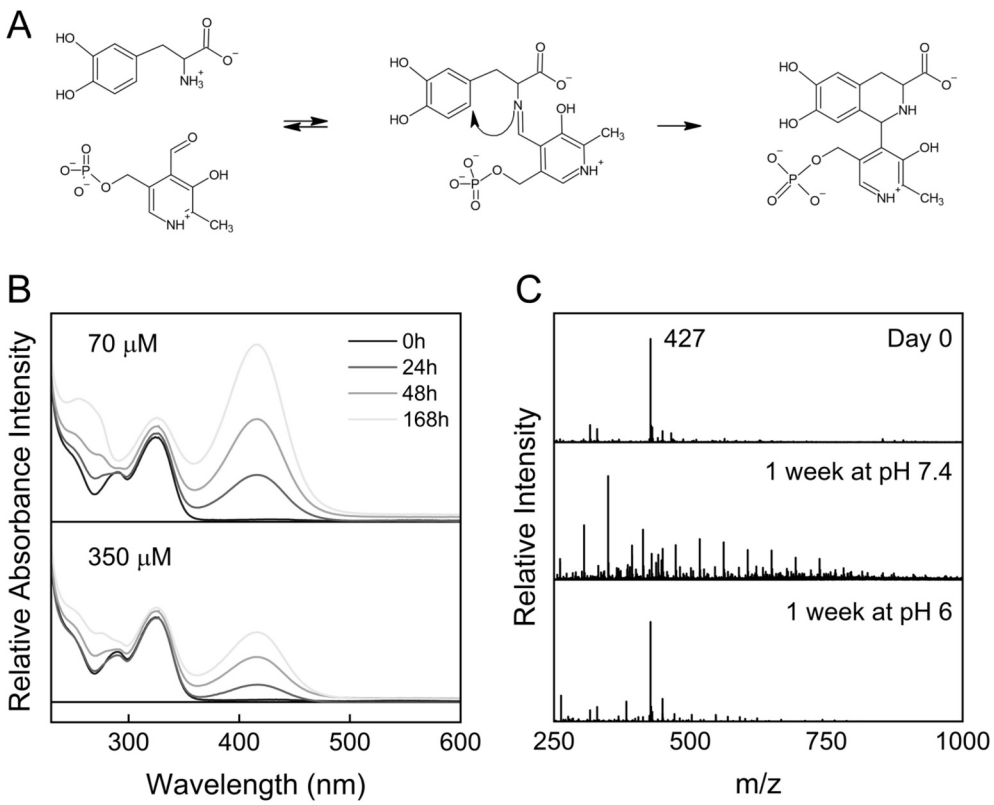


Fig. 3. Chemical characterization and pH-dependent stability of Pictet-Spengler adduct. (A) Schematic representation of the nonenzymatic Pictet–Spengler condensation between L-Dopa and PLP, yielding a cyclic adduct, through a Schiff base intermediate. **(B)** UV–Vis absorption spectra of the cyclic adduct at 70 μM (top) and 350 μM (bottom) incubated in sodium phosphate buffer (pH 7.4) for increasing times (0, 24, 48, and 168 h). UV–Vis data are reported in the same scale. The progressive appearance of an absorption band at ~420 nm and visible yellowing of the solution indicate the formation of oxidized and/or polymeric species. **(C)** Mass spectra of freshly prepared adduct (top), adduct incubated for one week at pH 7.4 (center), and adduct incubated for one week at pH 6 (bottom). Incubation at physiological pH results in heterogeneous polymeric species, whereas the cyclic adduct remains chemically stable under mildly acidic conditions.

driven oxidative pathways analogous to those underlying dopamine melanogenesis [34]. In contrast, both oxidation and polymerization are strongly suppressed at pH 6 (Fig. 3C**, bottom)**, where catechol groups remain largely protonated and chemically stable. Taken together, these observations indicate that the pH- and concentration-dependent spectral changes of the Pictet-Spengler adduct reflect the transient accumulation of catechol-derived oxidation intermediates that are rapidly consumed through secondary reactions, rather than a simple increase in overall oxidation.

3.4. Syn aggregation is inhibited by the Pictet-Spengler adduct

To investigate the effect of Pictet-Spengler adduct on Syn aggregation, the compound was added to protein solutions at pH 7.4 and pH 6 using Syn/adduct molar ratios of 1:1 and 1:5 **(**Fig. 4A,B). Aggregation kinetics were monitored by ThT fluorescence, while TEM was used to evaluate aggregate morphology. At pH 7.4, where the cyclic adduct is chemically unstable, Syn fibrillation was inhibited in a dose-dependent manner. TEM images collected after 168 h show the presence of mature fibrils in samples containing Syn alone (Fig. 4E), whereas samples incubated with Pictet-Spengler adduct at a 1:5 ratio predominantly contained smaller, oligomeric species (Fig. 4F). In contrast, at pH 6, where the adduct remains chemically stable, no inhibition of fibrillation was observed, with ThT fluorescence intensities more than twofold higher than those measured at pH 7.4. The presence of large aggregated species in Syn-only samples and smaller oligomeric species in the presence of the Pictet-Spengler adduct was further confirmed by DLS measurements (Fig. 4C**).** Far UV CD spectroscopy revealed that the Pictet-Spengler adduct does not induce β-sheet formation in monomeric Syn over time, but rather stabilizes a disordered conformational ensemble distinct from that of the native monomer (Fig. 4D). When aggregation experiments were performed in the presence of catalase (**Fig. S1**), which scavenges reactive oxygen species and prevents Syn oxidation, no differences in aggregation kinetics were observed relative to control samples, and a dose-dependent inhibition of fibrillation was retained. This indicates that oxidation of Syn is not required for the observed inhibition, suggesting that chemically unstable species derived from Pictet-Spengler adduct, rather than the adduct itself or oxidative modification of the protein, are responsible for the altered aggregation behavior. Collectively, these results indicate that Pictet-Spengler adduct-mediated inhibition of Syn fibrillation is closely linked to its chemical instability at physiological pH.

To further characterize the molecular nature of Syn species formed during incubation, samples containing Syn alone or Syn with the adduct at 1:1 and 1:5 ratios were analyzed by RP-HPLC at 0, 48, and 168 h (Fig. 5). At pH 7.4, additional peaks eluting before native Syn appeared over time in Pictet-Spengler adduct-containing samples and were identified by mass spectrometry as oxidized Syn species (Table 3**).** This effect was more pronounced at a 1:5 ratio, where Syn molecules bearing up to four oxidative modifications were detected. In contrast, under moderate acidic conditions (pH 6), only unmodified Syn was observed by mass spectrometric analysis. These findings indicate that the chemical instability of the Pictet-Spengler compound not only correlates with fibrillation inhibition but also promotes progressive oxidation of Syn, which may contribute to the accumulation of smaller, oligomeric species.

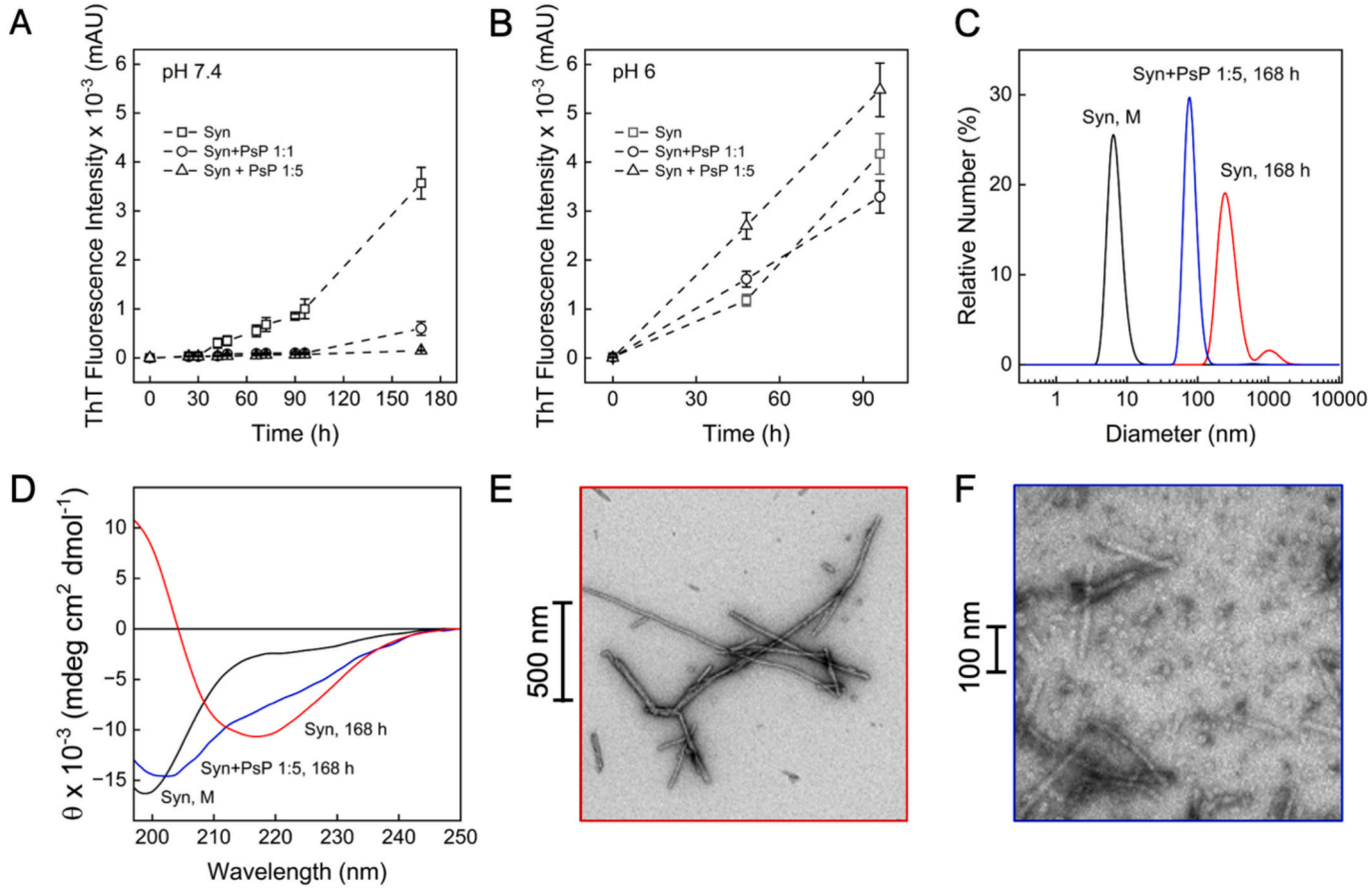


Fig. 4. Effect of the Pictet-Spengler adduct on Syn aggregation kinetics and aggregate morphology. (A, B) ThT fluorescence monitoring fibril formation of Syn alone (squares) or in the presence of adduct at 1:1 (circles) and 1:5 (triangles) molar ratios, incubated under aggregating conditions in sodium phosphate buffer at pH 7.4 **(A)** and pH 6 **(B)**. Data are reported as the mean value of three replicates ± SD. **(C)** Hydrodynamic radius of aggregation end-point species measured by DLS after 168 h. Data on particle size are reported as mean ± SD of a triplicate, each one consisting of 30 repetitions. **(D)** Far UV CD spectra of monomeric Syn before incubation (black), aggregates formed after 168 h in the absence of Pictet-Spengler adduct (red), and species formed in the presence of Pictet-Spengler adduct (1:5) (blue), showing reduced β-sheet content upon Pictet-Spengler adduct treatment. **(E, F)** Representative TEM micrographs of Syn aggregates formed after 168 h in the absence **(E)** or presence **(F)** of Pictet-Spengler adduct (1:5), revealing mature fibrils in control samples and predominantly smaller, less ordered species in Pictet-Spengler adduct -treated samples. PsP, Pictet-Spengler adduct. (For interpretation of the references to colour in this figure legend, the reader is referred to the web version of this article.)

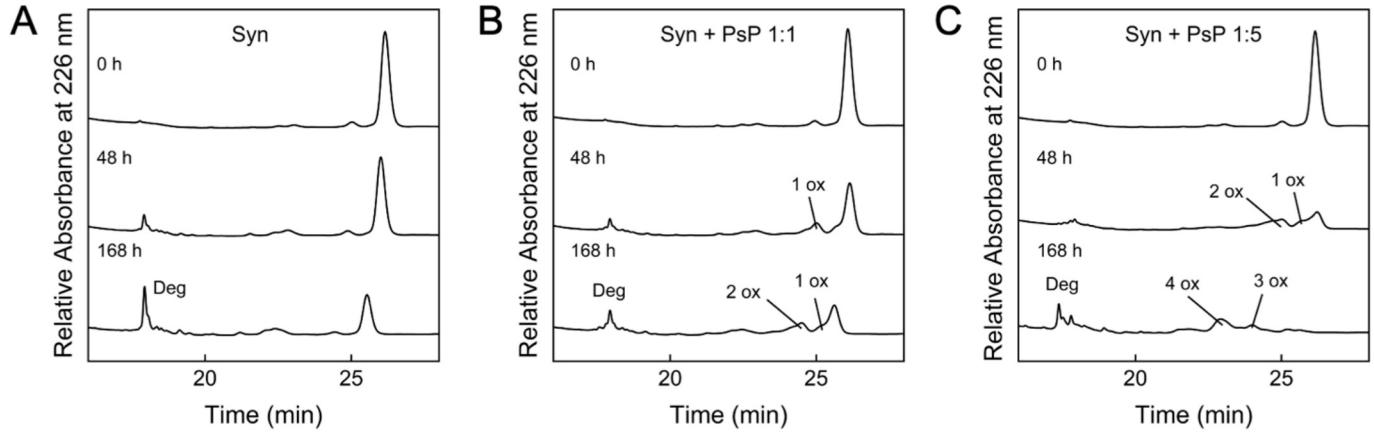


Fig. 5. Oxidative modification of Syn induced by Pictet-Spengler adduct during incubation. RP-HPLC chromatograms of Syn alone **(A)** or incubated with the adduct at 1:1 **(B)** and 1:5 **(C)** molar ratios at pH 7.4 for 0 h (top), 24 h (center), and 168 h (bottom). Additional peaks eluting before native Syn increase over time and with increasing Pictet-Spengler adduct concentration and were identified by mass spectrometry as oxidized Syn species. Oxidative modifications are absent under conditions in which the adduct is chemically stable (pH 6, not shown). Deg, species derived from degradation; ox, oxidized species of Syn; the number indicates the extent of modification; PsP, Pictet-Spengler adduct.

Table 3
Chemical characterization of the protein material corresponding to the major peaks in the chromatograms shown in Fig. 5. The adduct refers to the Pictet-Spengler condensation cyclic adduct.

Sample	Time	RT[a] (min)	Experimental Mass[b] (Da)	Species
Syn	0 h	25.6	14,459.04 ± 0.03	Syn
Syn + adduct	48 h	25.1	14,475.12 ± 0.19	Syn + 1 ox[c]
Syn + adduct	48 h	25.0	14,491.97 ± 0.22	Syn + 2 ox
Syn + adduct	168 h	23.9	14,508.08 ± 0.11	Syn + 3 ox
Syn + adduct	168 h	22.9	14,524.35 ± 0.09	Syn + 4 ox

[a] RT, RP-HPLC retention time.
[b] mass determined by ESI-MS.
[c] ox, Syn containing a Δmass of +16 Da due to one to four methionine residue (s) oxidation.

3.5. Interaction of Syn with the Pictet-Spengler adduct probed by native MS and ITC

Native MS provides insight into the conformational ensemble of Syn by analyzing its charge-state distribution under non-denaturing conditions, which reflects interconversion between distinct conformational states [17]. In this framework, lower *m/z* values correspond to more extended conformations due to increased solvent exposure of protonatable groups. At 0 h (Fig. 6A,B), Syn alone displays three interconverting conformational populations, corresponding to extended, intermediate, and compact states. Upon addition of the Pictet-Spengler adduct at 0 h, the populations corresponding to the most extended and most compact conformations markedly decrease in favor of the intermediate state (Fig. 6A,B), suggesting a redistribution of the conformational ensemble and a kinetic stabilization of this intermediate conformation. Despite this, no complex between the adduct and Syn was detectable. Interestingly, the small molecule was still detected in the native MS spectrum after SEC purification of the protein (**Fig. S2**). This indicates that any interactions between Syn and the adduct do not persist through transfer to the gas phase, even under native MS conditions. Nevertheless, despite the absence of a detectable complex, the adduct clearly alters the conformational landscape of Syn.

ITC measurements (Fig. 6C) were performed to further characterize this interaction and revealed a thermogram with negligible enthalpic contribution, consistent with the absence of a stable, specific binding event. Together with the native MS data, these results suggest that the observed conformational rearrangement is driven by weak, non-specific interactions that are predominantly entropic in nature. One possible explanation is a transient hydrophobic interaction between the adduct and the non-amyloid component region of Syn (amino acids 61–95), leading to compaction in solution. Such interactions are expected to be lost during ionization and gas-phase transfer, where hydrophobic effects are abolished and electrostatic interactions dominate [35], providing a plausible explanation for the lack of detectable Syn–adduct complexes by native MS.

3.6. Cytotoxicity of Syn formed in the presence of the Pictet-Spengler adduct

Notably, the Pictet-Spengler adduct alone did not exhibit cytotoxicity toward SH-SY5Y cells, causing only a modest (~10%) reduction in cell viability at the highest concentration tested (350 μM). (Fig. 7A). Given that the Pictet-Spengler adduct stabilizes Syn in fibril-incompetent, oligomeric states, we next assessed the cytotoxicity of Syn species formed in the presence of the cyclic compound. Syn incubated alone for 48 h (oligomer-enriched) or 168 h (fibril-enriched) induced moderate toxicity in SH-SY5Y cells following 24 h exposure (75 and 88% cell viability) (Fig. 7B). In contrast, Syn samples generated in the presence of the Pictet-Spengler adduct for the same incubation times did not induce detectable cytotoxicity under these conditions. Interestingly, upon prolonged exposure (48 h), Syn-adduct samples exhibited toxicity comparable to that of Syn oligomers and fibrils, although a bit lower (Fig. 7C). The initial absence of toxicity followed by a delayed onset, in contrast to Syn alone which displays toxicity already at early time points, suggests that the Pictet-Spengler adduct may modulate the interaction of Syn assemblies with cells. In particular, the adduct may slow down the cellular uptake or membrane interaction of toxic Syn species, thereby delaying the manifestation of cytotoxic effects.

4. Discussion

This study identifies a connection between the structural impairments of AADC and the generation of a chemically reactive metabolite capable of modulating Syn behavior. Specifically, we show that a subset of catalytically affected AADC deficiency variants promotes the formation of the Pictet–Spengler cyclic adduct between L-Dopa and PLP, a reaction that is negligible in the WT enzyme. The Pictet–Spengler condensation effectively converts the enzyme-bound cofactor into a dead-end product, irreversibly depleting PLP from the active site. These findings may have potential therapeutic implications. Vitamin B_6 (pyridoxine, precursor of PLP) supplementation is currently recommended as a treatment for AADC deficiency [11], and raises the possibility that it may enhance the propensity of some variants to undergo this unproductive reaction, under conditions in which L-Dopa level increases, due to the metabolic block caused by the genetic variants.

The ability of the AADC variants to produce the cyclic adduct appears to be tightly linked to structural perturbations affecting the active

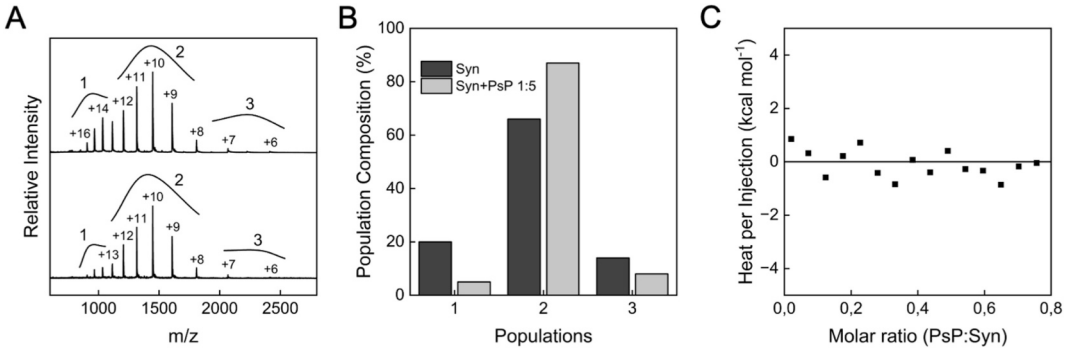


Fig. 6. Probing the interaction between the Pictet-Spengler adduct and Syn. (A) Native mass spectra of Syn alone (top) and Syn upon the addition of adduct at a 1:5 M ratio (bottom). Charge-state distributions reveal a shift toward more compact conformational populations upon the Pictet-Spengler compound addition. **(B)** Quantification of extended and compact conformer populations for Syn alone (black) and in the presence of the Pictet-Spengler adduct (grey), showing an increase in population 2 and decrease of 1 and 3. **(C)** ITC thermogram obtained by titrating the Pictet-Spengler adduct into Syn at pH 7.4, after subtraction of adduct dilution heat.
PsP, Pictet-Spengler adduct.

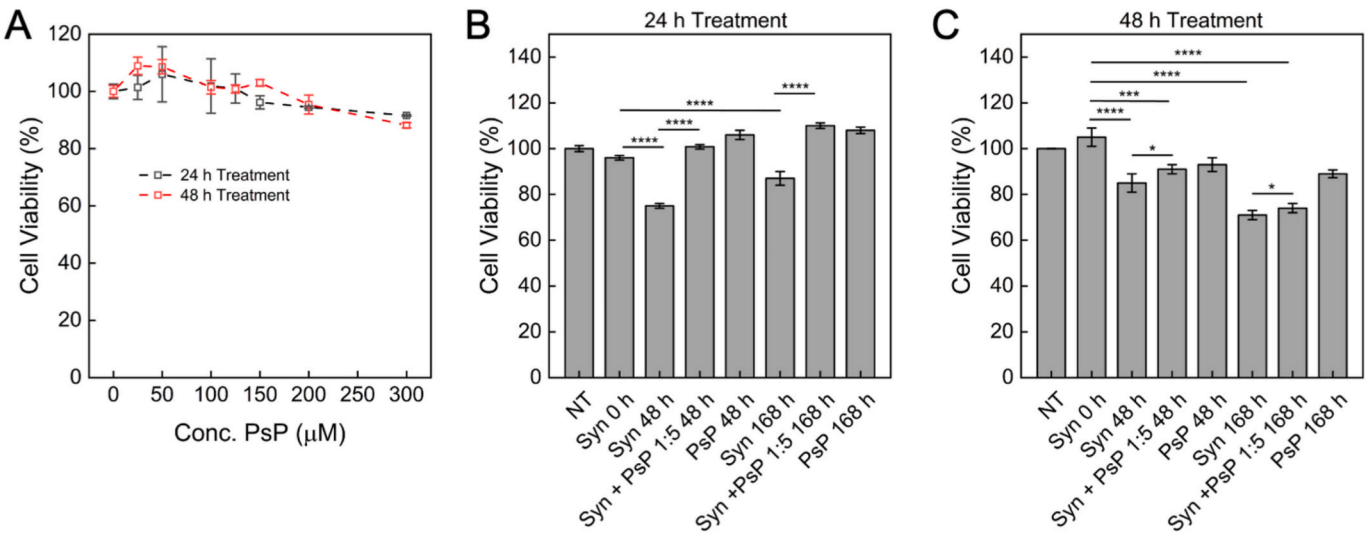


Fig. 7. Cellular effects of the Pictet-Spengler adduct alone or in the presence of Syn aggregates. (A) Cell viability of SH-SY5Y neuroblastoma cells treated with increasing concentrations of the Pictet-Spengler adduct (0–300 μM) for 24 h (black) and 48 h (red), measured by metabolic activity assay.
The viability of SH-SY5Y cells treated with Syn incubated for 48 h (oligomer enriched) and 168 h (fibril enriched) in further 24 h **(B)** or 48 h **(C)** time exposure in the absence or in the presence (1:5) of the Pictet-Spengler adduct. Abbreviation: NT, not treated; PsP, Pictet-Spengler adduct. $^{*}P < 0.05$, $^{***}P < 0.001$, $^{****}P < 0.0001$. (For interpretation of the references to colour in this figure legend, the reader is referred to the web version of this article.)

site. In the WT enzyme, PLP is maintained in a microenvironment that protects the cofactor from solvent exposure and undesired side reactions, as in all PLP-dependent enzymes [4]. By contrast, the investigated loss-of-function AADC variants can be classified into two groups: (i) variants resembling the WT, which do not produce significant amounts of the cyclic adduct, and (ii) variants that irreversibly convert PLP into the Pictet–Spengler product, with reaction rates significantly higher than the WT (Table 1). This distinction is based on several factors. First, *in silico* structural modeling shows that the variants mapping on loop3 (p.Pro330Leu, p.Arg347Gln and p.Leu353Pro) may affect the flexibility of this loop, preventing catalysis, without major structural crashes. Instead, the other variants are predicted to present structural impairments. Interestingly, structural dynamics of AADC regions far from the active site, has been demonstrated to be essential for the catalytic loop closure upon the active site [7], underscoring how the global structural integrity of the protein can trigger active site functionality. Second, we observed that the extent of the destabilization induced by the amino acid modifications is associated with a signal indicative of folding (Fig. 2B and Table 2). The higher the destabilizing effect, the lower the dichroic signal at 280 nm. Consistently, the same dichroic signals, indicative of alterations in the microenvironment of aromatic residues, correlate with the catalytic PLP center (Fig. 2C), indicating the association among subtle structural perturbations and cofactor microenvironment. Interestingly, the initial rate of the Pictet-Spengler condensation reaction correlates with the alteration of the dichroic signal at 280 nm (Fig. 2F) which, in turn, is correlated with the alteration of the cofactor binding mode. Notably, Ser147Arg and Phe309Leu, even if not so much compromised in folding, are able to synthesize the cyclic adduct at high rates, mainly due to the fact that their amino acid substitutions directly affect PLP and L-Dopa stabilization.

Notably, the Pictet–Spengler adduct has not previously been reported or investigated as a potential biomarker in AADC deficiency patient samples. Even though its formation or accumulation *in vivo* as well as its possible biological effects have not yet been directly demonstrated, further studies are required to assess its physiological relevance.

To explore the potential biological effects on biological macromolecules, we investigated Syn, a protein with a key role in Parkinson's Disease, as a target of the Pictet–Spengler adduct, due to its presynaptic localization and its established ability to interact with catechol-moieties [17–20]. Our results show that the Pictet–Spengler adduct inhibits Syn fibrillation in a dose-dependent manner and, under the same experimental conditions, promotes oxidative modification of the protein. Under the same conditions, the adduct is chemically unstable, as indicated by the progressive yellowing of the solution. Our previous studies demonstrated that catechol-containing compounds interact with Syn through both covalent and non-covalent mechanisms. These molecules stabilize Syn conformers that are otherwise prone to aggregation under equilibrium conditions in solution, thereby reducing their aggregation propensity. In addition, we showed that catechols attenuate the production of reactive oxygen species (ROS) induced by Syn aggregates and diminish their interaction with cellular membranes [17,19,29,36]. Given the structural similarity between the Pictet–Spengler adduct and other catechol-containing compounds, it is reasonable to propose that, similarly to these molecules, the adduct binds Syn through a combination of electrostatic interactions, mediated by its negatively charged group, and hydrophobic contacts involving its aromatic catechol ring. Such interactions may alter the long-range intramolecular contacts between the N- and C-terminal regions, as well as between the nonamyloid beta component (NAC) region and the C-terminus, which are known to play a key role in maintaining the conformational ensemble of monomeric Syn [37]. Perturbation of these long-range interactions could shift the conformational equilibrium toward species with reduced aggregation propensity, consistent with the effects previously reported for other catechol-containing molecules.

Control experiments indicate that hydrogen peroxide-dependent oxidation is not required for aggregation inhibition, as inhibition was maintained in the presence of catalase, whereas chemical instability appears to contribute to the inhibitory effect, as no inhibitory activity was observed at pH 6, where the adduct remains stable [17,19,38–41]. Therefore, we cannot exclude the possibility that one or more species generated during adduct decomposition contribute to the observed effects, as these products could not be isolated and characterized individually.

Syn exhibits a notable affinity for catechol-containing molecules, which can lead to diverse biological effects *in vivo* [42,43]. This interaction is particularly relevant because catechol compounds (such as dopamine, DOPAL, DOPAC, DOPET) can influence its functional properties [17,44]. Depending on the conditions, catechol binding can either inhibit fibril formation by stabilizing soluble intermediates or promote

the accumulation of modified oligomeric species. In addition, these interactions may alter neurotransmitter homeostasis by sequestering catechol molecules or promoting their oxidation, leading to the generation of reactive quinones. These reactive species can further modify Syn and other cellular components, potentially contributing to oxidative stress. Overall, the affinity of Syn for catechol-containing compounds suggests a dual role: it may exert protective effects under certain conditions by limiting aggregation, but it may also contribute to cellular dysfunction through the formation of toxic intermediates and disruption of normal biochemical pathways.

Overall, we propose that loss-of-function AADC variants with an altered PLP-binding site are prone to undergoing the nonenzymatic Pictet–Spengler condensation. The resulting product is not inert but may exert biological effects due to its pro-oxidant nature, thereby potentially modulating the disease phenotype. Importantly, this mechanism may extend beyond this early-onset non-progressive monogenic infantile Parkinsonism [23,45,46]. In patients with late-onset neurodegenerative Parkinson's Disease treated with L-Dopa, similar irreversible condensation reactions have been reported with reactive aldehydes or pyridoxine derivatives [21], possibly contributing to disease complexity. Although the adduct does not engage in specific molecular interactions with Syn, its chemical instability may contribute to the disruption of cellular redox balance, adding to the oxidative stress that drives Syn pathology.

CRediT authorship contribution statement

Philipp Trolese: Writing – review & editing, Writing – original draft, Investigation, Formal analysis, Data curation. **Giovanni Bisello:** Writing – review & editing, Writing – original draft, Investigation, Formal analysis, Data curation, Conceptualization. **Cristian Andres Carmona Carmona:** Investigation, Formal analysis, Data curation. **Giulia Spagnoli:** Investigation, Formal analysis, Data curation. **Alberto Benetollo:** Investigation, Formal analysis, Data curation. **Doriana Sandonà:** Investigation, Formal analysis, Data curation. **Laura Acquasaliente:** Writing – review & editing, Formal analysis, Data curation. **Patrizia Polverino de Laureto:** Writing – review & editing, Validation, Supervision, Project administration, Conceptualization. **Mariarita Bertoldi:** Writing – review & editing, Validation, Supervision, Project administration, Conceptualization.

Funding sources

MB acknowledges FUR2025 grant of the University of Verona and PRIN2022 code 2022BTMTP8, National Recovery and Resilience Plan (NRRP) funded by the Ministero dell'Università e della Ricerca (MUR).

Declaration of competing interest

The authors declare that they have no competing financial interests or personal relationships that could have appeared to influence the work reported in this paper.

Acknowledgements

Spectroscopic measurements were carried out at the “Centro Piattaforme Tecnologiche” of the University of Verona. We are thankful to the Mass Spectrometry Facility of Department of Pharmaceutical and Pharmacological Science, and Imaging Facility of Department of Biology, at University of Padova, for technical support.

Appendix A. Supplementary data

Supplementary data to this article can be found online at https://doi.org/10.1016/j.ijbiomac.2026.153968.

Data availability

Data will be made available on request.

References

[1] E.A. Rudd, W.C. Cunningham, J.W. Thanassi, Coenzyme–substrate adducts as inhibitors of mouse liver 3,4-dihydroxyphenylalanine decarboxylase, J. Med. Chem. 22 (3) (1979) 233–237.
[2] M. Bertoldi, P. Frigeri, M. Paci, C.B. Voltattorni, Reaction specificity of native and nicked 3,4-dihydroxyphenylalanine decarboxylase, J. Biol. Chem. 274 (9) (1999) 5514–5521.
[3] R. Montioli, G. Bisello, M. Dindo, G. Rossignoli, C.B. Voltattorni, M. Bertoldi, New variants of AADC deficiency expand the knowledge of enzymatic phenotypes, Arch. Biochem. Biophys. 682 (2020) 108263.
[4] R.A. John, Pyridoxal phosphate-dependent enzymes, Biochim. Biophys. Acta 1248 (2) (1995) 81–96.
[5] M. Bertoldi, C. Borri Voltattorni, Reaction of dopa decarboxylase with L-aromatic amino acids under aerobic and anaerobic conditions, Biochem. J. 352 (Pt 2) (2000) 533–538.
[6] R. Montioli, B. Cellini, C. Borri Voltattorni, Molecular insights into the pathogenicity of variants associated with the aromatic amino acid decarboxylase deficiency, J. Inherit. Metab. Dis. 34 (6) (2011) 1213–1224.
[7] G. Bisello, R.P. Ribeiro, M. Perduca, B.D. Belviso, P. Polverino De' Laureto, A. Giorgetti, R. Caliandro, M. Bertoldi, Human aromatic amino acid decarboxylase is an asymmetric and flexible enzyme: implication in aromatic amino acid decarboxylase deficiency, Protein Sci. 32 (8) (2023) e4732.
[8] J. Nishino, H. Hayashi, S. Ishii, H. Kagamiyama, An anomalous side reaction of the Lys303 mutant aromatic L-amino acid decarboxylase unravels the role of the residue in catalysis, J. Biochem. 121 (3) (1997) 604–611.
[9] M. Bertoldi, S. Castellani, C. Bori Voltattorni, Mutation of residues in the coenzyme binding pocket of Dopa decarboxylase: effects on catalytic properties, Eur. J. Biochem. 268 (10) (2001) 2975–2981.
[10] M. Bertoldi, C.B. Voltattorni, Multiple roles of the active site lysine of Dopa decarboxylase, Arch. Biochem. Biophys. 488 (2) (2009) 130–139.
[11] T. Wassenberg, M. Molero-Luis, K. Jeltsch, G.F. Hoffmann, B. Assmann, N. Blau, A. Garcia-Cazorla, R. Artuch, R. Pons, T.S. Pearson, V. Leuzzi, M. Mastrangelo, P. L. Pearl, W.T. Lee, M.A. Kurian, S. Heales, L. Flint, M. Verbeek, M. Willemsen, T. Opladen, Consensus guideline for the diagnosis and treatment of aromatic l-amino acid decarboxylase (AADC) deficiency, Orphanet J. Rare Dis. 12 (1) (2017) 12.
[12] N. Himmelreich, M. Bertoldi, M. Alfadhel, M.A. Alghamdi, Y. Anikster, X. Bao, F. A. Bashiri, B.B. Zeev, G. Bisello, A.C. Ceylan, Y.H. Chien, Y.S. Choy, S.H. Elsea, L. Flint, A. Garcia-Cazorla, C. Gijavanekar, E.Y. Gumus, M.H. Hamad, B. Hismi, T. Honzik, O.K. Hubschmann, W.L. Hwu, S. Ibanez-Mico, K. Jeltsch, N. Julia-Palacios, C.S. Kasapkara, M.A. Kurian, K. Kusmierska, N. Liu, L.H. Ngu, J.D. Odom, W.P. Ong, T. Opladen, M. Oppeboen, P.L. Pearl, B. Perez, R. Pons, A.M. Rygiel, T. E. Shien, R. Spaull, J. Sykut-Cegielska, B. Tabarki, T. Tangeraas, B. Thony, T. Wassenberg, Y. Wen, Y. Yakob, J.G.C. Yin, J. Zeman, N. Blau, Prevalence of DDC genotypes in patients with aromatic L-amino acid decarboxylase (AADC) deficiency and in silico prediction of structural protein changes, Mol. Genet. Metab. 139 (3) (2023) 107624.
[13] R. Montioli, R. Battini, A. Paiardini, M. Tolve, M. Bertoldi, C. Carducci, V. Leuzzi, C. Borri Voltattorni, A novel compound heterozygous genotype associated with aromatic amino acid decarboxylase deficiency: clinical aspects and biochemical studies, Mol. Genet. Metab. 127 (2) (2019) 132–137.
[14] G. Bisello, K. Kusmierska, M.M. Verbeek, J. Sykut-Cegielska, M.A.A.P. Willemsen, R.A. Wevers, K. Szymańska, J. Poznanski, J. Drozak, K. Wertheim-Tysarowska, A. M. Rygiel, M. Bertoldi, The novel P330L pathogenic variant of aromatic amino acid decarboxylase maps on the catalytic flexible loop underlying its crucial role, Cell. Mol. Life Sci. 79 (6) (2022) 305.
[15] J.T. Bendor, T.P. Logan, R.H. Edwards, The function of alpha-synuclein, Neuron 79 (6) (2013) 1044–1066.
[16] R. Tehranian, S.E. Montoya, A.D. Van Laar, T.G. Hastings, R.G. Perez, Alpha-synuclein inhibits aromatic amino acid decarboxylase activity in dopaminergic cells, J. Neurochem. 99 (4) (2006) 1188–1196.
[17] B. Fongaro, E. Cappelletto, A. Sosic, B. Spolaore, P. Polverino de Laureto, 3,4-Dihydroxyphenylethanol and 3,4-dihydroxyphenylacetic acid affect the aggregation process of E46K variant of alpha-synuclein at different extent: insights into the interplay between protein dynamics and catechol effect, Protein Sci. 31 (7) (2022) e4356.
[18] I. Inciardi, E. Rizzotto, F. Gregoris, B. Fongaro, A. Sosic, G. Minervini, P. Polverino de Laureto, Catechol-induced covalent modifications modulate the aggregation tendency of alpha-synuclein: an in-solution and in-silico study, Biofactors 51 (1) (2025) e2086.
[19] L. Palazzi, B. Fongaro, M. Leri, L. Acquasaliente, M. Stefani, M. Bucciantini, P. Polverino de Laureto, Structural features and toxicity of alpha-Synuclein oligomers grown in the presence of DOPAC, Int. J. Mol. Sci. 22 (11) (2021).
[20] E. Rizzotto, A. Pierangelini, B. Fongaro, M. Leri, I. Inciardi, P. Trolese, V. De Filippis, M. Bucciantini, L. Acquasaliente, P. Polverino de Laureto, DOPAC as a modulator of alpha-Synuclein and E46K interactions with membrane: insights into binding dynamics, Int. J. Biol. Macromol. 294 (2025) 139427.
[21] M. Sandler, S.B. Carter, K.R. Hunter, G.M. Stern, Tetrahydroisoquinoline alkaloids: in vivo metabolites of L-dopa in man, Nature 241 (5390) (1973) 439–443.

[22] M.G. Spillantini, M.L. Schmidt, V.M. Lee, J.Q. Trojanowski, R. Jakes, M. Goedert, Alpha-synuclein in Lewy bodies, Nature 388 (6645) (1997) 839–840.
[23] R. Pons, T.S. Pearson, B. Perez-Duenas, A. Garcia-Cazorla, M.A. Kurian, Z. Dalivigka, V. Zouvelou, C. Outsika, E. Kokkinou, M. Sigatullina-Bondarenko, A. Darling, M.D.M. O'Callaghan, R. Spaull, D.B.D. Steel, E. Salamou, M.J. Forjaz, C. Rodriguez-Blazquez, Development and preliminary validation of a parkinsonism-dystonia scale for infants and young children, Mov. Disord. 40 (8) (2025) 1669–1679.
[24] C.A. Carmona-Carmona, G. Bisello, R. Franchini, G. Lunardi, R. Galavotti, M. Perduca, R.P. Ribeiro, B.D. Belviso, A. Giorgetti, R. Caliandro, P.M. Lievens, M. Bertoldi, The CRISPR-Cas9 knockout DDC SH-SY5Y in vitro model for AADC deficiency provides insight into the pathogenicity of R347Q and L353P variants: a cross-sectional structural and functional analysis, FEBS J. 292 (18) (2025) 4833–4853.
[25] J. Delgado, L.G. Radusky, D. Cianferoni, L. Serrano, FoldX 5.0: working with RNA, small molecules and a new graphical interface, Bioinformatics 35 (20) (2019) 4168–4169.
[26] C.H.M. Rodrigues, D.E.V. Pires, D.B. Ascher, DynaMut2: assessing changes in stability and flexibility upon single and multiple point missense mutations, Protein Sci. 30 (1) (2021) 60–69.
[27] D.E. Pires, D.B. Ascher, T.L. Blundell, DUET: a server for predicting effects of mutations on protein stability using an integrated computational approach, Nucleic Acids Res. 42 (Web Server issue) (2014) W314–W319.
[28] J. Abramson, J. Adler, J. Dunger, R. Evans, T. Green, A. Pritzel, O. Ronneberger, L. Willmore, A.J. Ballard, J. Bambrick, S.W. Bodenstein, D.A. Evans, C.C. Hung, M. O'Neill, D. Reiman, K. Tunyasuvunakool, Z. Wu, A. Zemgulyte, E. Arvaniti, C. Beattie, O. Bertolli, A. Bridgland, A. Cherepanov, M. Congreve, A.I. Cowen-Rivers, A. Cowie, M. Figurnov, F.B. Fuchs, H. Gladman, R. Jain, Y.A. Khan, C.M. R. Low, K. Perlin, A. Potapenko, P. Savy, S. Singh, A. Stecula, A. Thillaisundaram, C. Tong, S. Yakneen, E.D. Zhong, M. Zielinski, A. Zidek, V. Bapst, P. Kohli, M. Jaderberg, D. Hassabis, J.M. Jumper, Accurate structure prediction of biomolecular interactions with AlphaFold 3, Nature 630 (8016) (2024) 493–500.
[29] L. Palazzi, M. Leri, S. Cesaro, M. Stefani, M. Bucciantini, P. Polverino de Laureto, Insight into the molecular mechanism underlying the inhibition of alpha-synuclein aggregation by hydroxytyrosol, Biochem. Pharmacol. 173 (2020) 113722.
[30] S.M. Kelly, T.J. Jess, N.C. Price, How to study proteins by circular dichroism, Biochim. Biophys. Acta 1751 (2) (2005) 119–139.
[31] R. Montioli, M. Dindo, A. Giorgetti, S. Piccoli, B. Cellini, C.B. Voltattorni, A comprehensive picture of the mutations associated with aromatic amino acid decarboxylase deficiency: from molecular mechanisms to therapy implications, Hum. Mol. Genet. 23 (20) (2014) 5429–5440.
[32] D. Sulzer, L. Zecca, Intraneuronal dopamine-quinone synthesis: a review, Neurotox. Res. 1 (3) (2000) 181–195.
[33] N. Umek, B. Gersak, N. Vintar, M. Sostaric, J. Mavri, Dopamine autoxidation is controlled by acidic pH, Front. Mol. Neurosci. 11 (2018) 467.
[34] D. Sulzer, J. Bogulavsky, K.E. Larsen, G. Behr, E. Karatekin, M.H. Kleinman, N. Turro, D. Krantz, R.H. Edwards, L.A. Greene, L. Zecca, Neuromelanin biosynthesis is driven by excess cytosolic catecholamines not accumulated by synaptic vesicles, Proc. Natl. Acad. Sci. USA 97 (22) (2000) 11869–11874.
[35] C.V. Robinson, E.W. Chung, B.B. Kragelund, J. Knudsen, R.T. Aplin, F.M. Poulsen, C.M. Dobson, Probing the nature of noncovalent interactions by mass spectrometry. A study of protein−CoA ligand binding and assembly, J. Am. Chem. Soc. 118 (36) (1996) 8646–8653.
[36] L. Palazzi, E. Bruzzone, G. Bisello, M. Leri, M. Stefani, M. Bucciantini, P. Polverino de Laureto, Oleuropein aglycone stabilizes the monomeric alpha-synuclein and favours the growth of non-toxic aggregates, Sci. Rep. 8 (1) (2018) 8337.
[37] P. Kumari, D. Ghosh, A. Vanas, Y. Fleischmann, T. Wiegand, G. Jeschke, R. Riek, C. Eichmann, Structural insights into alpha-synuclein monomer-fibril interactions, Proc. Natl. Acad. Sci. USA 118 (10) (2021).
[38] F.E. Herrera, A. Chesi, K.E. Paleologou, A. Schmid, A. Munoz, M. Vendruscolo, S. Gustincich, H.A. Lashuel, P. Carloni, Inhibition of alpha-synuclein fibrillization by dopamine is mediated by interactions with five C-terminal residues and with E83 in the NAC region, PLoS One 3 (10) (2008) e3394.
[39] D. Dibenedetto, G. Rossetti, R. Caliandro, P. Carloni, A molecular dynamics simulation-based interpretation of nuclear magnetic resonance multidimensional heteronuclear spectra of alpha-synuclein.Dopamine adducts, Biochemistry 52 (38) (2013) 6672–6683.
[40] O. Tavassoly, S. Nokhrin, O.Y. Dmitriev, J.S. Lee, Cu(II) and dopamine bind to alpha-synuclein and cause large conformational changes, FEBS J. 281 (12) (2014) 2738–2753.
[41] M.K. Jain, R. Bhat, Modulation of human alpha-synuclein aggregation by a combined effect of calcium and dopamine, Neurobiol. Dis. 63 (2014) 115–128.
[42] J.R. Mazzulli, A.J. Mishizen, B.I. Giasson, D.R. Lynch, S.A. Thomas, A. Nakashima, T. Nagatsu, A. Ota, H. Ischiropoulos, Cytosolic catechols inhibit alpha-synuclein aggregation and facilitate the formation of intracellular soluble oligomeric intermediates, J. Neurosci. 26 (39) (2006) 10068–10078.
[43] T. Zohoorian-Abootorabi, A.A. Meratan, S. Jafarkhani, V. Muronetz, T. Haertle, A. A. Saboury, Modulation of cytotoxic amyloid fibrillation and mitochondrial damage of alpha-synuclein by catechols mediated conformational changes, Sci. Rep. 13 (1) (2023) 5275.
[44] L. Guan, L. Lin, C. Ma, L. Qiu, Decoding crosstalk between neurotransmitters and alpha-synuclein in Parkinson's disease: pathogenesis and therapeutic implications, Ther. Adv. Neurol. Disord. 18 (2025) 17562864251339895.
[45] R. Pons, The phenotypic spectrum of paediatric neurotransmitter diseases and infantile parkinsonism, J. Inherit. Metab. Dis. 32 (3) (2009) 321–332.
[46] V. Leuzzi, F. Nardecchia, R. Pons, S. Galosi, Parkinsonism in children: clinical classification and etiological spectrum, Parkinsonism Relat. Disord. 82 (2021) 150–157.